Earth and Planetary Science Letters 438 (2016) 103–111

Contents lists available at ScienceDirect

Earth and Planetary Science Letters

www.elsevier.com/locate/epsl

Oxygen-17 anomaly in soil nitrate: A new precipitation proxy for desert landscapes

Fan Wang [a], Wensheng Ge [b], Hao Luo [c], Ji-Hye Seo [c], Greg Michalski [a,c,*]

[a] Department of Earth, Atmospheric and Planetary Sciences, Purdue University, 550 Stadium Mall Drive, West Lafayette, IN, USA
[b] School of Earth Sciences and Resources, China University of Geosciences (Beijing), No. 29 Xueyuan Road, Haidian District, Beijing, China
[c] Department of Chemistry, Purdue University, 560 Oval Drive, West Lafayette, IN, USA

ARTICLE INFO

Article history:
Received 27 April 2015
Received in revised form 26 December 2015
Accepted 2 January 2016
Available online xxxx
Editor: M. Frank

Keywords:
desert nitrate
oxygen-17 anomaly
mass-independent isotopic fractionation
precipitation proxy
climate

ABSTRACT

The nitrogen cycle in desert soil ecosystems is particularly sensitive to changes in precipitation, even of relatively small magnitude and short duration, because it is already under water stress. This suggests that desert soils may have preserved past evidence of small variations in continental precipitation. We have measured nitrate (NO_3^-) concentrations in soils from the Atacama (Chile), Kumtag (China), Mojave (US), and Thar (India) deserts, and stable nitrogen and oxygen isotope (^{15}N, ^{17}O, and ^{18}O) abundances of the soil NO_3^-. ^{17}O anomalies ($\Delta^{17}O$), the deviations from the mass-independent isotopic fractionation, were detected in soil NO_3^- from almost all sites of these four deserts. There was a strong negative correlation between the mean annual precipitation (MAP) and soil NO_3^- $\Delta^{17}O$ values ($\Delta^{17}O_{NO_3soil}$). This MAP-$\Delta^{17}O_{NO_3soil}$ correlation advocated $\Delta^{17}O_{NO_3soil}$ as a new precipitation proxy and was then used to assess precipitation changes in southwestern US at the Pliocene–Pleistocene boundary, in South America during the Miocene, and the Sahara Desert in the past 10 kyr using NO_3^- $\Delta^{17}O$ in paleosols or ancient aquifers. Global and the US maps of surface $\Delta^{17}O_{NO_3soil}$ were also projected with available MAP datasets based on the MAP-$\Delta^{17}O_{NO_3soil}$ model.

1. Introduction

Nitrate (NO_3^-) is often the dominant form of fixed nitrogen in desert soils (Ericksen, 1981; Walvoord et al., 2003; Graham et al., 2008), but the mechanisms leading to its accumulation remain uncertain. NO_3^- accrues naturally via atmospheric deposition and *in situ* biological nitrification (Boring et al., 1988). Atmospheric deposition of NO_3^- occurs through both wet deposition of dissolved NO_3^- in rain, snow, and fog, and dry deposition of aerosol NO_3^- and gaseous nitric acid (Seinfeld and Pandis, 2006). In water-limited desert regions, the wet deposition rate can be proportional to local mean annual precipitation (MAP), while the dry deposition may also be a function of MAP (Seinfeld and Pandis, 2006). Nitrification, the oxidation of ammonia/ammonium into NO_3^- by microbes, is often the main source of NO_3^- in soils on Earth (Boring et al., 1988). The nitrification rates in desert soils are also, in part, controlled by MAP since low soil water contents can inhibit microbial activities by lowering intracellular water (Gleeson et al., 2008). The relative importance of these two sources in desert soils, deposition versus nitrification, and their dependences on MAP, however, are poorly constrained over space and time (Boring et al., 1988; Walvoord et al., 2003).

Oxygen isotope abundances have recently proven useful for distinguishing these two NO_3^- sources (Michalski et al., 2004). Oxygen consists of three stable isotopes: ^{16}O, ^{17}O and ^{18}O. For the majority of material and processes on Earth, there exist isotopic fractionations that are proportional to the relative differences in isotope masses and these are referred as mass-dependent isotopic fractionations (see review in Thiemens, 2006). During nitrification, oxygen atoms of water and air that both comply with the mass-dependent law are proportionally transferred to NO_3^-, which itself is a mass-dependent process, leading to $\delta^{17}O \approx 0.52 \cdot \delta^{18}O$ in biotic NO_3^- (Miller, 2002). Atmospheric NO_3^-, on the other hand, contains an "anomalous" ^{17}O excess over what is expected based on ^{18}O abundances (Michalski et al., 2003). The deviation from mass-dependent fractionation is called "mass-independent isotopic fractionation" and quantified by $\Delta^{17}O = \delta^{17}O - 0.52 \bullet \delta^{18}O$ (Miller, 2002; Thiemens, 2006). The $\Delta^{17}O$ values of atmospheric NO_3^- ($\Delta^{17}O_{NO_3atm}$) have been observed to range from 20–35‰ (Michalski et al., 2003; Alexander et al., 2009; Morin et al., 2009),

* Corresponding author at: Department of Earth, Atmospheric and Planetary Sciences, Purdue University, 550 Stadium Mall Drive, West Lafayette, IN, USA. Tel.: +1 7654943704; fax: +1 7654961210.
E-mail address: gmichals@purdue.edu (G. Michalski).

http://dx.doi.org/10.1016/j.epsl.2016.01.002
0012-821X/

which arises during NO_x oxidation by tropospheric ozone that has $\Delta^{17}O$ values of 25–35‰ (Michalski and Bhattacharya, 2009; Vicars and Savarino, 2014). Soil NO_3^- $\Delta^{17}O$ ($\Delta^{17}O_{NO_3soil}$) values can then be used to apportion the two NO_3^- sources by applying a two-component $\Delta^{17}O$ mixing model:

$$\Delta^{17}O_{NO_3soil} = f_{atm} \bullet \Delta^{17}O_{NO_3atm} + f_{nitrif} \bullet \Delta^{17}O_{NO_3nitrif} \quad (1)$$

where $\Delta^{17}O_{NO_3nitrif}$ is the $\Delta^{17}O$ value of soil NO_3^- produced from nitrification that is approximately zero, and f_{atm} and f_{nitrif} are the mole fractions of atmospheric deposition and nitrification contributing to the soil NO_3^- pool, respectively ($f_{atm} + f_{nitrif} = 1$) (Michalski et al., 2004; Dejwakh et al., 2012). Since atmospheric NO_3^- deposition and nitrification rates are both sensitive to precipitation changes in desert regions, we hypothesize that MAP variations can alter f_{atm} and f_{nitrif} in different proportions and become manifested in $\Delta^{17}O_{NO_3soil}$. Thus $\Delta^{17}O_{NO_3soil}$ can serve as a MAP proxy in desert regions, where nitrification is sufficiently slow that it cannot completely override the NO_3^- accumulated by atmospheric NO_3^- deposition.

The connection between desert MAP and $\Delta^{17}O_{NO_3soil}$ has previously been noted. Rech et al. (2006) compared the $\Delta^{17}O_{NO_3soil}$ values in a 9 Ma paleosol stratum along the eastern margin of the Atacama Desert (Chile) with those in the Atacama's hyper-arid core to estimate MAP during the late Miocene. Ewing et al. (2007) demonstrated an increase in $\Delta^{17}O_{NO_3soil}$ along a relatively narrow precipitation transect (MAP: 21 mm to 2 mm) in the Atacama. However, there has been no detailed study evaluating how $\Delta^{17}O_{NO_3soil}$ varies with precipitation in deserts except the Atacama. Here we present the $\Delta^{17}O_{NO_3soil}$ data of four globally distributed deserts and a calibration of $\Delta^{17}O_{NO_3soil}$ versus MAP relationship, then highlight the use of $\Delta^{17}O_{NO_3soil}$ as a precipitation proxy for inferring MAP in past climate states, and ultimately project the global and US overviews of $\Delta^{17}O_{NO_3soil}$ based on available MAP datasets.

2. Soil sampling and analysis

Undisturbed soils were collected from 22 sites in four hot deserts (Atacama, Chile; Kumtag, China; Mojave, United States; and Thar, India) (Fig. 1, Table 1). The Atacama Desert, located between the Coastal Range to the west and the Andes to the east in northern Chile, is one of the driest places on Earth with modern-time MAP <2 mm in its hyper-arid core (Houston, 2006b). It is well known to contain massive NO_3^- deposits in the world that have been extensively mined since early 1800s (Ericksen, 1981). The Kumtag Desert is located in the Turpan-Hami Basin in western China, which is the second-driest and the only inland desert among these four deserts with typical MAP of 30–50 mm in most areas (Li et al., 2011). 2.5 billion ton NO_3^- deposits, rivaling those in the Atacama, have recently been identified in the Kumtag (Qin et al., 2012). The Mojave Desert is situated in southwestern US between the Great Basin Desert to the north and the Sonoran Desert to the south with typical MAP of 30–300 mm (Hereford et al., 2006). Sporadic subsurface (~2 m) NO_3^- deposits have been found in the Mojave (Walvoord et al., 2003; Graham et al., 2008). The Thar Desert, located in northwestern India forming a natural boundary along the border between India and Pakistan, is wettest among the four deserts with typical MAP of 100–500 mm (Pramanik, 1952). NO_3^- deposits in the Thar have not been documented, but sufficient NO_3^- was found in soils analyzed in this study for oxygen isotope analysis.

Sampling sites on stable and ancient landforms with typical desert surfaces were selected also based on the distinction from mining excavations and roads as well as the availability of MAP data in order to span a wide range of MAP rates. Decadal MAP data of nearby meteorological stations were obtained for the Atacama sites from Houston (2006b), Kumtag sites from Li et al. (2011), and Thar sites from Indian National Data Center, while MAP data for the Mojave sites were interpolated using the PRISM model (http://oldprism.nacse.org). At most of these sites, the soil was mantled by desert pavement, a common land-surface feature in desert regions. Patchy bushes were found at some sites (see detailed site descriptions in SI Table S1), and only the open space between bushes was sampled. All soil profiles were hand sampled from the surface to a depth of 20–50 cm. Samples were stored in air-tight plastic bags at 20°C until analysis.

Bulk soils were first sieved using 2 mm sieves. 1–20 g of the sieved soil was added to 30–40 ml of Millipore water and the soil–water mixture was vortexed to extract water soluble salts. NO_3^- concentrations ($[NO_3^-]$) were measured by Dionex DX-500 ion chromatography. The sieved Kumtag soils were weighed of ~2 mg into tin capsules that are loaded to the Sercon (Crewe, UK) GLS elemental analyzer-Hydra 20/22 isotope ratio mass spectrometer (EA-IRMS) system for $\delta^{15}N$ analysis. The measurement of our laboratory working references NC32 yielded $\delta^{15}N$ of 15.3 ± 0.3‰. The NC32 was mixed by the potassium nitrate (KNO_3) obtained from North Carolina State University (NCSU, prepared by equilibrating water and reagent grade HNO_3 per Böhlke et al., 2003) and USGS32 ($\delta^{15}N = 180‰$) in the ratio of 93:7. The sample run was also calibrated by international references of NIST 1547 peach leave ($\delta^{15}N = 1.5‰$), USGS34 ($\delta^{15}N = -1.8‰$) and USGS35 ($\delta^{15}N = 2.7‰$). Meanwhile, the sieved soils from the Kumtag and Thar were extracted of NO_3^- that was then purified by removing sulfate salts, converted into $AgNO_3$, and thermally decomposed with the resulting O_2 analyzed by Delta (Thermo Fisher, US) V Plus IRMS (Michalski et al., 2004). The $\delta^{18}O$ and $\Delta^{17}O$ precision were both ±0.2‰ obtained by replicate analysis of our $\Delta^{17}O$ = 19.8‰ laboratory working reference (20H) that was the purified Hoffman nitrate fertilizer (Hi-Yield Nitrate of Soda) mined from ore deposits in the Atacama. Instead, samples from the Atacama and Mojave were analyzed of $\delta^{15}N$, $\delta^{18}O$ and $\Delta^{17}O$ simultaneously using a recent bacterial reduction and gold redox method (Kaiser et al., 2007). Six laboratory NO_3^- working references with $\Delta^{17}O = 0$, 1‰, 2‰, 5‰, 10‰ and 19.8‰ were run to generate duplicate calibration curves and for quality control, showing precision for $\delta^{15}N$, $\delta^{18}O$ and $\Delta^{17}O$ of ±0.4‰, ±1‰ and ±0.5‰, respectively (Riha, 2013). The $\Delta^{17}O = 0$ working reference NC32 and $\Delta^{17}O = 19.8‰$ working reference 20H were described above, and four other working references were made by appropriately mixing NC32 and 20H (Riha, 2013). All working references were previously calibrated using international NO_3^- isotope references, *i.e.* USGS32 ($\delta^{18}O = 25.7‰$), USGS34 ($\delta^{18}O = -14.8‰$, $\Delta^{17}O = 0$) and USGS35 ($\delta^{18}O = 51.5‰$, $\Delta^{17}O = 21.1‰$). All $\delta^{15}N$ values were reported versus air N_2 and oxygen values ($\delta^{18}O$, $\Delta^{17}O$) were reported with respect to VSMOW. All analyses were conducted at the Purdue Stable Isotope Facility.

3. Results and discussion

3.1. NO_3^- concentrations and isotopic signatures

$[NO_3^-]$ were highest in Kumtag soils ranging from 3.8–94.0 μmol/(g soil), typically one order of magnitude higher than those from the Atacama (0.2–8.5 μmol/(g soil)) or the Mojave (0.2–3.3 μmol/(g soil)) (Table 1). This is because all the Kumtag sites were located in major mining areas where nitrate deposits of high ore grades were reported to have mainly accumulated in the surface or subsurface (15–70 cm) (Qin et al., 2012), while the sites in other deserts were in non-mining or mine tailing areas. Further data analysis indicated that the Atacama soil $[NO_3^-]$ were a power

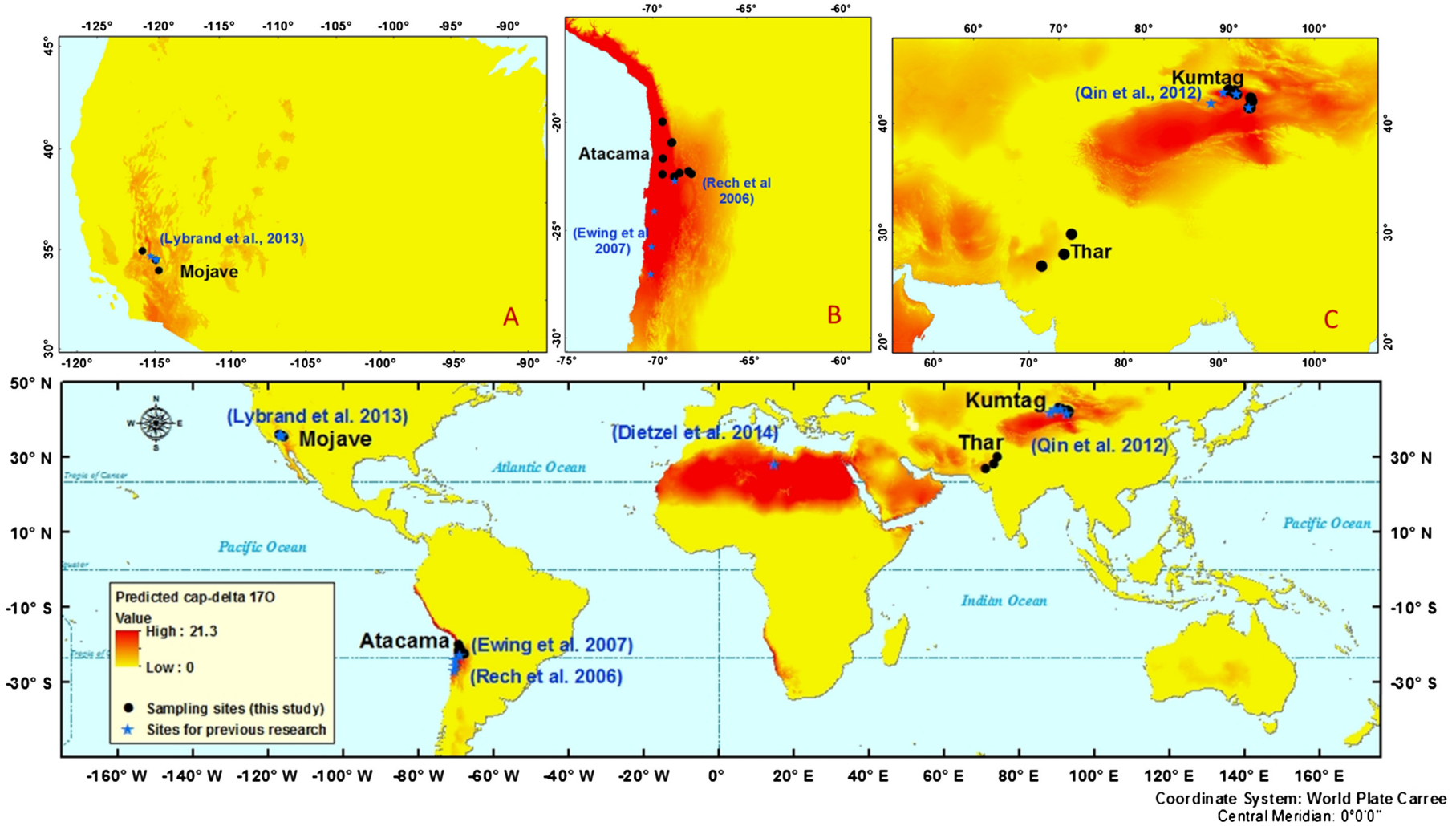

Fig. 1. Bottom: the predicted global distribution of surface $\Delta^{17}O_{NO_3soil}$ between 50°N and 50°S based on the MAP-$\Delta^{17}O_{NO_3soil}$ model (inverted Eq. (2): $\Delta^{17}O_{NO_3soil} = -8.28\ln(MAP) + 45.8$) with global MAP data from http://www.worldclim.org; upper (A): the predicted surface $\Delta^{17}O_{NO_3soil}$ around the USA with MAP data of higher-resolution from http://www.prism.oregonstate.edu/; upper (B) and (C): the zoom-in pictures of the $\Delta^{17}O_{NO_3soil}$ distribution in South America and Asia continents, respectively.

Table 1
Precipitation gradient site information and the concentration and isotopic data.

Sampling site	Coordinates (elevation, m)	MAP (mm)	Sampling depth (cm)	Average $[NO_3^-]$[a] (μmol/(g soil))	$\delta^{15}N_{NO_3\,soil}$ (‰) $\pm 1\sigma$ (n[b])	$\delta^{18}O_{NO_3\,soil}$ (‰) $\pm 1\sigma$ (n)	$\Delta^{17}O_{NO_3\,soil}$ (‰) $\pm 1\sigma$ (n)
Atacama Desert, Chile							
Calama	22.53°S 68.97°W (4374)	4.2	0–20	0.8	$-4.3 \pm 0.7(2)$[c]	$44.9 \pm 2.9(2)$[c]	$16.0 \pm 1.9(2)$[c]
Chiu Chiu	22.34°S 68.66°W (2555)	4.4	0–25	0.9	$-1.1 \pm 0.4(2)$[c]	$38.1 \pm 9.0(3)$[c]	$19.1 \pm 0.6(3)$[c]
Copaquire	20.94°S 69.07°W (3384)	54.1	0–20	0.6	5.9(1)[c]	29.1(1)[c]	9.6(1)[c]
Coya Sur	22.40°S 69.58°W (1220)	0.4	0–30	6.5	$-1.9 \pm 0.6(4)$[c]	$47.2 \pm 3.6(4)$[c]	$21.3 \pm 1.4(4)$[c]
El Tatio	22.38°S 68.02°W (4374)	153.9	0–30	0.2	$5.3 \pm 12.3(1)$[c]	$38.0 \pm 3.0(2)$[c]	$6.1 \pm 8.6(2)$[c]
Huatacondo	20.92°S 69.04°W (2219)	11.5	0–50	1.7	$-10.4 \pm 3.7(2)$[c]	$52.8 \pm 1.0(2)$[c]	$20.6 \pm 1.5(2)$[c]
Ojos	19.96°S 69.54°W (1336)	0.9	0–20	3.0	7.1(1)[d]	$38.1 \pm 1.3(2)$[e]	$16.2 \pm 0.5(2)$[e]
Quillagua	21.68°S 69.54°W (906)	0.2	0–10	8.5	$-3.2 \pm 0.4(2)$[c]	$46.6 \pm 1.0(2)$[c]	$19.7 \pm 0.5(2)$[c]
Tocene	22.26°S 68.19°W (3237)	94.1	0–40	N.A.	14.4(1)[c]	22.1(1)[c]	5.1(1)[c]
Kumtag Desert, China							
Dananhu	42.37°N 92.82°E (543)	40.5	0–30	20.6	$3.3 \pm 0.6(7)$[d]	$47.6 \pm 1.8(7)$[e]	$16.5 \pm 0.5(7)$[e]
Dawadi	41.45°N 92.65°E (1028)	49.1	0–30	21.9	6.5(1)[d]	55.1(1)[e]	14.4(1)[e]
Kumtag mine	42.69°N 91.17°E (312)	36.5	0–30	59.2	6.3(1)[d]	47.4(1)[e]	$16.3 \pm 0.2(2)$[e]
Kuzishan	41.45°N 92.80°E (1079)	49.1	0–10	94.0	$10.8 \pm 0.8(2)$[d]	$44.5 \pm 1.2(2)$[e]	$12.3 \pm 0.2(2)$[e]
Qiketai	42.92°N 90.88°E (408)	36.5	0–20	3.8	1.5(1)[d]	44.5(1)[e]	17.5(1)[e]
Xiaocaohu	43.10°N 90.30°E (713)	36.5	0–50	5.1	2.1(1)[d]	39.8(1)[e]	17.6(1)[e]
Xigebi	42.05°N 92.95°E (767)	40.5	0–30	11.6	$5.4 \pm 0.3(2)$[d]	$41.5 \pm 2.0(2)$[e]	$14.9 \pm 0.5(2)$[e]
Mojave Desert, USA							
Cima	35.20°N 115.87°W (1106)	149.9	0–30	0.2	$0.9 \pm 1.7(4)$[c]	$23.7 \pm 1.0(4)$[c]	$7.4 \pm 0.5(4)$[c]
Lower canyon	35.71°N 116.23°W (217)	90.7	0–30	N.A.	15.1(1)[c]	48.9(1)[c]	9.3(1)[c]
Pannemint	36.03°N 117.30°W (469)	106.2	0–43	3.3	$0.9 \pm 2.2(3)$[c]	$27.6 \pm 2.3(3)$[c]	$11.1 \pm 0.6(3)$[c]
Thar Desert, India							
Bikaner	28.05°N 73.24°E (215)	305.0	0–50	N.A.	N.A.	15.2(1)[e]	0.3(1)[e]
Ganganagar	29.87°N 73.89°E (176)	200.0	0–50	N.A.	N.A.	12.0(1)[e]	1.2(1)[e]
Jaisalmer	26.94°N 70.94°E (218)	212.0	0–50	N.A.	N.A.	$11.0 \pm 0.2(2)$[e]	$0.4 \pm 0.2(2)$[e]

N.A.: not applicable because not measured.
[a] For sites with sub-samples from different depths, the concentrations were depth weighed average concentrations.
[b] Sample replicates for the same site.
[c] Measured by bacterial reduction method.
[d] Measured by the EA-IRMS system.
[e] Measured by thermal decomposition method.

function of MAP ($[NO_3^-] = 3.0 \bullet MAP^{-0.5}$, $r^2 = 0.88$), evidencing that drier climates are more advantageous for nitrate accumulation. However, this $[NO_3^-]$-MAP relationship was not significant for the Mojave or Kumtag soils. This suggested that NO_3^- accumulation varied in different deserts and was also affected by geographic differences. We suspect that the wettest Thar, where the sampled ~10 g soils were only sufficient for $\delta^{18}O$ and $\Delta^{17}O$ analysis without the $[NO_3^-]$ and $\delta^{15}N$ data, had the lowest soil $[NO_3^-]$ among the four deserts.

The Atacama sites had soil NO_3^- $\delta^{15}N$ ($\delta^{15}N_{NO_3soil}$) and $\delta^{18}O$ ($\delta^{18}O_{NO_3soil}$) values of −10.4–14.4‰ and 22.1–52.8‰, respectively (Table 1). These values spanned broader ranges compared to those reported for the Atacama sites by Böhlke et al. (1997) and Michalski et al. (2004), probably owing to that this study covered more climatic zones and non-mining areas. While $\delta^{15}N_{NO_3soil}$ does not vary significantly between potential sources and cannot be used to distinguish different sources with certainty, high $\delta^{18}O_{NO_3soil}$ values were usually ascribed to atmospheric deposition that usually has NO_3^- $\delta^{18}O$ values of 40–70‰ (Böhlke et al., 1997; Michalski et al., 2004). In this study, low $\delta^{18}O_{NO_3soil}$ values (<40‰) associated with positive $\delta^{15}N_{NO_3soil}$ occurred in high-altitude sites with high MAP rates (El Tatio, Tocene and Copaquire), as well as the northernmost Ojos site, probably suggesting the terrestrial sources of NO_3^- (nitrification). The negative correlation between $\delta^{15}N_{NO_3soil}$ and $\delta^{18}O_{NO_3soil}$ for the Atacama ($\delta^{15}N_{NO_3soil} = -0.7\delta^{18}O_{NO_3soil} + 27.3$, $r^2 = 0.89$) may also suggest the mixing of NO_3^- from atmospheric and terrestrial sources. The high $\delta^{18}O_{NO_3soil}$ values (39.8–55.1‰) for the Kumtag sites were also likely due to the atmospheric origin. The Kumtag $\delta^{15}N_{NO_3soil}$ values (1.5–10.8‰) were for bulk soils, but consistent with those for NO_3^- reported for the same sites by Qin et al. (2012), suggesting NO_3^- is the major form of nitrogen in Kumtag soils. The highest $\delta^{15}N_{NO_3soil}$ values were found in Kuzishan (10.8‰) and Dawadi (6.5‰), two sites with salt lake-type deposits of niter (KNO_3), while the other Kumtag sites with caliche-type deposits of sodium niter ($NaNO_3$) had low $\delta^{15}N$ values of 1.5–6.3‰ (Table 1). This is in agreement with the discovery by Qin et al. (2012) that the isotopic compositions were mineralogically different, but we did not observe lower $\delta^{18}O_{NO_3soil}$ values in salt lake-type deposits compared to the caliche-type deposits in our study as suggested by Qin et al. (2012). The $\delta^{15}N_{NO_3soil}$ and $\delta^{18}O_{NO_3soil}$ were not correlated in the Kumtag. The Cima and Pannemint sites had similar $\delta^{15}N_{NO_3soil}$ (0–4.8‰) and $\delta^{18}O_{NO_3soil}$ (21.3–36.0‰) values to those for the Mojave reported in Böhlke et al. (1997) and Michalski et al. (2004), but the Lower canyon site had significantly higher $\delta^{15}N_{NO_3soil}$ (15.1‰) and $\delta^{18}O_{NO_3soil}$ (48.9‰) values than previously reported values (Table 1). As far as we know, the $\delta^{15}N_{NO_3soil}$ and $\delta^{18}O_{NO_3soil}$ of the Thar Desert are hereby reported for the first time.

The soil NO_3^- $\Delta^{17}O$ ($\Delta^{17}O_{NO_3soil}$) of the 22 sites across four deserts varied from 0.3–21.3‰ (Table 1). The largest $\Delta^{17}O_{NO_3soil}$ values were observed in hyper-arid regions (MAP < 50 mm, UNEP, 1997) of the Atacama (16.0–21.3‰) and the Kumtag (12.3–17.6‰), indicating the major origin of soil NO_3^- from atmospheric deposition that is consistent with the inference from the $\delta^{18}O_{NO_3soil}$. In the arid regions (50 < MAP < 200 mm, UNEP, 1997) of the Mojave as well as some high-altitude sites in the Atacama, the $\Delta^{17}O_{NO_3soil}$ values were significantly lower (5.1–11.1‰), which suggested the increasing importance of nitrification to the soil NO_3^- pool. The lowest $\Delta^{17}O_{NO_3soil}$ of 0–1‰ occurred in the semi-arid Thar (200 < MAP < 500 mm, UNEP, 1997), suggesting the shift in the origin of soil NO_3^- to predominantly nitrification.

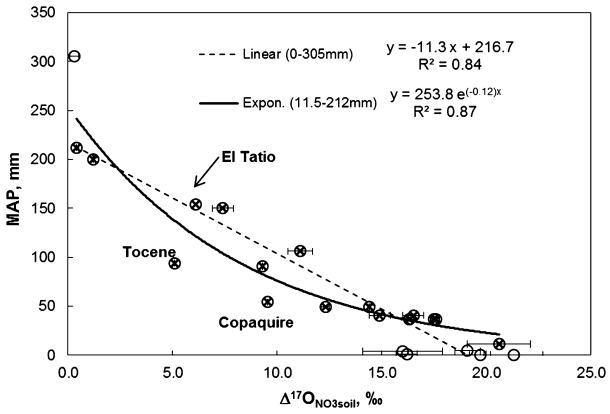

Fig. 2. Regression of the MAP against $\Delta^{17}O_{NO_3soil}$ ($\pm 1\sigma$). The dashed line indicates regression for the total dataset (hollow circles), while the solid line is regression for the data points with MAP of 11.5–212 mm (*x* cross).

3.2. The derivation of $\Delta^{17}O_{NO_3soil}$ as a precipitation proxy

Further, the $\Delta^{17}O_{NO_3soil}$ showed a linear dependence on MAP over the sampling site MAP range of 0.4–305 mm: $MAP = -11.3 \bullet \Delta^{17}O_{NO_3soil} + 216.7$ ($r^2 = 0.84$) (Fig. 2), suggesting the potential of $\Delta^{17}O_{NO_3soil}$ as a MAP proxy. However, there are upper and lower limits of MAP after which the $\Delta^{17}O_{NO_3soil}$ proxy becomes invalid for precipitation inference. The upper limit of MAP would correspond to the analytical detection limit of $\Delta^{17}O_{NO_3soil}$ of 0.5‰. This upper limit (MAP ~ 210 mm) is reached in the Jaisalmer area of the Thar where nitrification has outpaced atmospheric NO_3^- deposition, with only ~2% contribution of atmospheric NO_3^- to total soil NO_3^- budget based on Eq. (1) using the modern-time average $\Delta^{17}O_{NO_3atm}$ value of ~ 23‰ (Michalski et al., 2003). The lower limit of MAP occurs where atmospheric deposition is the only NO_3^- input source in the soil. When MAP = 0, there should be no nitrification contributing to soil NO_3^-, and the MAP-$\Delta^{17}O_{NO_3soil}$ equation indicates $\Delta^{17}O_{NO_3soil} \sim 20$‰, close to the observed $\Delta^{17}O_{NO_3soil}$ of 20.6 ± 1.5‰ at the Huatacondo sites (MAP = 11.5 mm), suggesting a $\Delta^{17}O_{NO_3soil}$ plateau likely occurring when MAP = 11.5 mm. Therefore, approximately 11.5 mm can be the dry end of microbial activities below which nitrification is nearly eliminated, as nitrification (and $\Delta^{17}O_{NO_3soil}$) can vary strongly with small increases in MAP (Fig. 2). 11.5 mm is then set as the lower limit of MAP that can be determined by the $\Delta^{17}O_{NO_3soil}$ proxy. $\Delta^{17}O_{NO_3soil}$ values from sites with MAP rates between that of Huatacondo and Jaisalmer, i.e. 11.5–212 mm, were then used to recalibrate the MAP-$\Delta^{17}O_{NO_3soil}$ relationship. After comparison, an exponential function (Fig. 2) was adopted:

$$MAP = 253.8 \exp(-0.12 \bullet \Delta^{17}O_{NO_3soil}) \ (r^2 = 0.87) \quad (2)$$

This significant correlation between MAP and $\Delta^{17}O_{NO_3soil}$ advocates that $\Delta^{17}O_{NO_3soil}$ can work as a MAP proxy for ancient nitrate deposits with the applicable range of 11.5–212 mm.

Beyond these application limits, we acknowledge that there are also some uncertainties inherent in the $\Delta^{17}O_{NO_3soil}$ proxy. The first uncertainty in the MAP-$\Delta^{17}O_{NO_3soil}$ relationship arises from using the modern-time precipitation data to represent the precipitation information over the timescales of soil NO_3^- accumulation that may span geological periods. However, precipitation records before 1900 A.D., especially in desert regions, are rarely available. Therefore, the existing decade-scale precipitation data (Table 1) were used to constrain the relationship between MAP and $\Delta^{17}O_{NO_3soil}$, but the uncertainty was minimized by only using surface or near-surface (<50 cm) soils that would represent NO_3^- that has recently accumulated.

The second uncertainty in the MAP-$\Delta^{17}O_{NO_3soil}$ model is that $\Delta^{17}O_{NO_3atm}$ was assumed constant but indeed may have varied between different sites or over time at the same site (Eq. (1)), complicating the direct derivation of the MAP-$\Delta^{17}O_{NO_3soil}$ relationship. Observations (Michalski et al., 2003) and isotope models (Alexander et al., 2009) have shown that $\Delta^{17}O_{NO_3atm}$ values are determined mainly by the oxidation capacity (the interaction of three principal oxidants in the lower atmosphere O_3, •OH and H_2O_2). All the four studied deserts are geographically similar (mid-latitude, bounded by mountain ranges, high temperatures, high actinic flux, low biogenic emissions) and their spatial extents are relatively small. Therefore, the oxidation capacity in each desert that controls $\Delta^{17}O_{NO_3atm}$ values is not likely to be significantly different. Temporal variations of $\Delta^{17}O_{NO_3atm}$ also cannot be significant for using the MAP-$\Delta^{17}O_{NO_3soil}$ proxy because these variations would average out over the NO_3^- accumulation timescales (100–1000 yrs) (Walvoord et al., 2003; Michalski et al., 2004). The modulation of annual $\Delta^{17}O_{NO_3atm}$ values by long-term accumulation is exemplified in recent analysis of dust collected for 2.5 years along an east-west transect in the Atacama (Wang et al., 2014). The $\Delta^{17}O$ values of NO_3^- extracted from the seven dust collectors located in the hyper-arid core (~160 km wide) were relatively consistent of 25.8 ± 0.5‰ (Wang et al., 2014), in contrast to the annual $\Delta^{17}O_{NO_3atm}$ variations of ~ 10‰ for an Andean ice core (Buffen et al., 2014). For its secular variations, the 30-year running average of the $\Delta^{17}O_{NO_3atm}$ values for the Site A, Greenland ice core during 1680=-1830 only showed a 2.5‰ variation, with the high values mainly owing to an elevation of O_3 and decrease of •OH in the atmosphere induced by the intense biomass burning recorded in North America (Alexander et al., 2004). Over the longer NO_3^- accumulation timescales (100–1000 yr), the $\Delta^{17}O_{NO_3atm}$ variations should be even smaller, especially considering additional processes such as physical mixing at the soil surface might further homogenize the temporal and spatial differences in the $\Delta^{17}O_{NO_3atm}$. Besides, the $\Delta^{17}O_{atm}$ variations in mid-latitude deserts are still difficult to resolve because of the great challenges in reconstructing oxidation chemistry, especially for ancient times. Therefore, no correction for the $\Delta^{17}O_{NO_3atm}$ effects was made during the derivation of the MAP-$\Delta^{17}O_{NO_3soil}$ relationship.

Thirdly, sampling issues may also account for some small uncertainties when applying the MAP-$\Delta^{17}O_{NO_3soil}$ proxy. To reduce sampling biases, replicates were collected from different depths (but <50 cm as discussed above) or locations at some sites and these typically showed only small differences in $\Delta^{17}O_{NO_3soil}$ (< 1‰). However, two sites showed significant $\Delta^{17}O_{NO_3soil}$ variations with location or depth. The El Tatio site is hilly (elevation > 4000 m, SI Table S1), and the $\Delta^{17}O_{NO_3soil}$ value of 12.1‰ for the sample from the hilltop is significantly larger than the $\Delta^{17}O_{NO_3soil}$ of zero for the sample from the hill slope (0–20 cm integrated sample). This is probably because water was unevenly distributed over the hill with the hill slope receiving and holding a significant amount of water drained from the hilltop, which was evident from the shrub coverage on the hill slope and barren surface with desert pavements on the hilltop (SI Table S1). Therefore, the average $\Delta^{17}O_{NO_3soil}$ of 6.1‰ for the two locations was used to calibrate the MAP-$\Delta^{17}O_{NO_3soil}$ relationship. The Copaquire site is a valley surrounded by mountains, and its $\Delta^{17}O_{NO_3soil}$ values are 9.6‰ at 0–3 cm and 3.3‰ at 10–20 cm. The significant disparity between these two different depths may indicate a wetter climate in ancient times when possible surface runoff brought in NO_3^- from other sources featured by lower $\Delta^{17}O_{NO_3soil}$ values or ancient water availability could sustain more *in situ* nitrification. To correspond to the modern-time precipitation data, the surface 0–3 cm $\Delta^{17}O_{NO_3soil}$ was adopted. However, the $\Delta^{17}O_{NO_3soil}$ of 9.6‰ is still low compared to the $\Delta^{17}O_{NO_3soil}$ at other sites with similar MAP (Fig. 2), probably due to that the Copaquire site that is subject to drain water from the surrounding mountains, different from most of other sites where precipitation is the major water source. The Tocene site, located in a mountain basin with 40% bush coverage (SI Table S1), also had a lower $\Delta^{17}O_{NO_3soil}$ (5.1‰) than expected, suggesting the possibly similar existence of drain water from mountains.

Fourthly, the model-data deviations might also arise if there were variations in evaporation between sites that might have influenced the $\Delta^{17}O_{NO_3soil}$ by varying the extents of microbial nitrification. Pan evaporation rates generally far exceed the actual evaporation because of the water limits in desert regions. For example, the recorded annual pan evaporation for our sites in the Atacama were 1984–3631 mm (Houston, 2006a), ~3000 mm in the Kumtag (Qin et al., 2012), and ~2000 mm in the Mojave (Blaney, 1957), which were similar in values between deserts but typically one or two orders of magnitude higher than their local MAP. Obviously, these desert evaporation potentials could not be fulfilled, and the local actual evaporation should approximate to local precipitation. Therefore, evaporation was not treated as an independent factor and thus not corrected for variations when deriving the MAP-$\Delta^{17}O_{NO_3soil}$ relationship. However, the typical vertical distribution of nitrate, chloride, and sulfate with increasing depths in the Kumtag suggested that soluble salts were up-drawn by capillary force and evaporation to precipitate in the sequence of solubility from salt-enriched ground water in the Kumtag, though the nitrate all mainly originated from atmospheric deposition (Qin et al., 2012). This "bottom–up" mechanism of shallow nitrate deposit formation is clearly different from the "top–down" infiltration mechanism occurring in the Atacama that induced the concentration of nitrate at depth and below sulfate (Ericksen, 1981). Nevertheless, we did not think that the difference in reconcentration mechanism could ruin the MAP-$\Delta^{17}O_{NO_3soil}$ relationship, though the $\Delta^{17}O_{NO_3soil}$ in the Kumtag might reflect the isotopic signatures of NO_3^- and precipitation information averaged over a larger groundwater-influenced area.

3.3. *Evaluating the MAP-$\Delta^{17}O_{NO_3soil}$ calibration*

The MAP-$\Delta^{17}O_{NO_3soil}$ calibration was evaluated by comparing our estimates with other published $\Delta^{17}O_{NO_3soil}$ values and regional precipitation records. Qin et al. (2012) measured the $\Delta^{17}O_{NO_3soil}$ of several NO_3^- deposits ranging from 5.9‰ to 20.7‰ in the Turpan–Hami basin in northwestern China (see sites in Fig. 1). Their wider $\Delta^{17}O_{NO_3soil}$ range than our measurements is mainly owing to those sites that did not overlap with our sites. The highest $\Delta^{17}O_{NO_3soil}$ of 20.7‰ yields an estimate of the MAP of 21.2 mm, which is similar to their reported average MAP of 15 mm for the Turpan–Hami basin and that of 17.3 mm for its nearby Turpan weather station (Li et al., 2011). The lowest value of 5.9‰ suggests a MAP of 125.0 mm, typical of precipitation in the local mountain range (Li et al., 2011). This supports the authors' proposed mechanism that the deposits are a mixture of local (hyper-arid) and remote (semi-arid) NO_3^- sources that are connected through a groundwater system.

Ewing et al. (2007) reported average $\Delta^{17}O_{NO_3soil}$ values of 17.1‰, 13.8‰, and 9.3‰ for three sites on Pliocene landforms along a south–north MAP transect in the Atacama (see sites in Fig. 1). Though Ewing et al. were among the first who recognized the control of $\Delta^{17}O_{NO_3soil}$ by MAP, they mainly focused on the transformation of soil nitrogen cycle from the nitrogen input and loss balance with mainly organic nitrogen in arid regions to inorganic nitrogen (mostly NO_3^-) accumulation and storage in hyper-arid regions as reflected by nitrogen species concentrations and NO_3^- isotope data along the MAP transect. Their data over a narrow precipitation transect were also insufficient to

develop a robust MAP-$\Delta^{17}O_{NO_3soil}$ relationship that can be used for paleoprecipitation estimation, but should be ideal for testing our MAP-$\Delta^{17}O_{NO_3soil}$ model. The $\Delta^{17}O_{NO_3soil}$ values by Ewing et al. (2007) would correspond to MAP of 32.6, 48.4 and 83.1 mm based on Eq. (2), which are significantly higher than the observed modern-time MAP of <2, 10, and 21 mm. There are two possible explanations for these discrepancies. First, most of these were subsurface NO_3^- (>50 cm deep) including older NO_3^- that was possibly formed under a wetter climate than the modern-time rainfall regime. A better comparison would be to only consider the surface NO_3^-. The $\Delta^{17}O_{NO_3soil}$ values of 19.4 ± 0.1‰ in the surface 1-3 cm layer at the MAP < 2 mm site (Yungay) by Ewing et al. (2007) is near the lower MAP limit of the $\Delta^{17}O_{NO_3soil}$ proxy, suggesting the MAP < 11.5 mm for the driest site, close to the observed <2 mm. There were no surface $\Delta^{17}O_{NO_3soil}$ data for the MAP = 10 mm and MAP = 21 mm sites but these can be inferred using the observed correlation of $\Delta^{17}O_{NO_3soil} = -3.4 + 0.43 \bullet \delta^{18}O_{NO_3soil}$ ($R^2 = 0.92$, Fig. 5 of Ewing et al., 2007). The surface 2 cm $\delta^{18}O_{NO_3soil}$ values were 49.9‰ at the MAP = 10 mm site and 43.8‰ for the MAP = 21 mm site, suggesting the surface $\Delta^{17}O_{NO_3soil}$ of 18.0‰ and 15.4‰ at the two sites, respectively. These values can yield MAP of 29.1 mm and 39.8 mm, closer to their MAP of 10 mm and 21 mm, respectively. The remaining discrepancies may then be due to the second possibility that fog plays a role in supplying water to nitrifying microbes. Intrusion of thick fogs through the Coastal Range into the inland sites in the Atacama is common (Cereceda and Schemenauer, 1991), and the deposited fog water may support sparse plant life and promote microbial activity (Warren-Rhodes et al., 2006). Thus, slightly higher predictions of MAP by our MAP-$\Delta^{17}O_{NO_3soil}$ proxy calibration compared to local precipitation data in coastal deserts could be due to fog precipitation being neglected from the local precipitation data.

3.4. Re-interpreting previous paleoclimate studies

The $\Delta^{17}O_{NO_3soil}$ proxy can be used to re-evaluate previously published paleoclimate interpretations for paleosols. However, NO_3^- salts are soluble, and can be mobilized within the soil profiles or leached into the ground water in the presence of small amounts of water. Large aqueous activities likely further mix and even homogenize NO_3^- from different sources or different depths, while wet periods may facilitate nitrification significantly to erase positive $\Delta^{17}O_{NO_3soil}$ legacies from previous dry periods. Therefore, cautions should be borne in mind when using the $\Delta^{17}O_{NO_3soil}$ proxy, and supplementary information (the site geological context and paleohydrology history evidences etc.), and additional analyses, such as the distribution of soluble salts that are indicative of dissolution and transport processes, are desired to help eventually decipher the climate information. Nevertheless, the robust MAP-$\Delta^{17}O_{NO_3soil}$ relationship for surface NO_3^- in desert regions suggested that aqueous activities or wet periods are not frequent to disturb the surface or subsurface NO_3^- preservation in some parts of desert regions. Hyper-aridity can further minimize the influences of aqueous events and help preserve NO_3^- at depth from mixing and leaching, which is exemplified by our previous research that heterogeneous $\Delta^{17}O_{NO_3soil}$ reflecting climate states in different periods were preserved in a ~2 m deep soil profile from the hyper-arid core of the Atacama (Wang, 2013). Therefore, at sites absent of large-scale hydrological impacts, coupling the $\Delta^{17}O_{NO_3soil}$ evidences with the interpretation of other geological and geochemical information can help guarantee the feasibility of the $\Delta^{17}O_{NO_3soil}$ proxy for paleoprecipitation inference. In addition, groundwater in deserts is widely known to have high concentrations of NO_3^- that is mainly from surface NO_3^- deposits (Dietzel et al., 2014). Since the recharge of desert groundwater is typically slow and not appreciable, ancient groundwater may also preserve paleoprecipitation information like paleosol, and the groundwater NO_3^- $\Delta^{17}O$ may then help constrain the paleoprecipitation.

Lybrand et al. (2013) measured $\Delta^{17}O_{NO_3soil}$ values of 7.0–13.2‰ of several clay hills in the southernmost region of Death Valley of the Mojave (see sites in Fig. 1). Those clay hills were covered with thin and blistered surface crusts and nearly absent of vegetation, while high contents of NO_3^- salts accumulate in "caliche" layers above the clay beds that were proposed to have moved in a "bottom–up" manner by capillary rise. It was postulated that these field sites were once playa or evaporating lakes that became desiccated after the Pleistocene and further buried and deformed by tectonic activities. After desiccation, biological soil crusts might be established with nitrate produced, while biotic and atmospheric nitrate from the surrounding areas could also be leached to the newly-exposed lake sediments. The $\Delta^{17}O_{NO_3soil}$ at the Sperry and Bully Hill sites were similar of 8.6 ± 0.2‰ and 7.3 ± 0.2‰, respectively, while the Confidence Hills site averaged 11.8 ± 2.0‰. These average $\Delta^{17}O_{NO_3soil}$ values yield a MAP of 61.6 mm for Confidence Hills, 90.4 mm for Sperry, and 105.7 mm for Bully Hill. Magneto stratigraphy suggested that the Confidence Hills formation was dated at late Pliocene, 2.14–2.15 Ma (Pluhar et al., 1991), and continued into the early Pleistocene (1.8 Ma) while Sperry and Bully Hill were younger than 1.8 Ma (Wright, 1974). This indicates that the Mojave was dry at 2.15 Ma (MAP ~50 mm), before transitioning to a wetter climate around 1.8 Ma. This is consistent with the relatively drier late Pliocene and Early Pleistocene inferred from compilation of proxy-based reconstructions in southwestern US (Thompson, 1991; Winnick et al., 2012) and then increased desiccation in the Holocene from an intermedite wet period (Walvoord et al., 2003). The advantage of our $\Delta^{17}O_{NO_3soil}$ proxy is its ability to quantify MAP during this dry-to-wet transition. The future improved positional age constraints on the Death Valley region may be used for higher resolution detection of MAP changes in southwestern US at the Pliocene–Pleistocene boundary.

$\Delta^{17}O_{NO_3soil}$ of 4.6–14.4‰ (mean 9.9‰) were determined by Rech et al. (2006) for the Barros Arana paleosol that was developed on basement rock or alluvial fan at elevations between 2200–3500 m along the southeastern margin of the Calama Basin of the Atacama (see sites in Fig. 1). The paleosol was estimated to have a minimum age of 9.4 Ma from ignimbrite dating. High concentrations of near-surface sulfates and chlorides and nitrates at depth as well as large vertical salt fractures were identified, which were not likely formed by capillary migration but the downward translocation of salt enriched dust into the profile during rare precipitation events (known as the "top–down" formation mechanism). Rech et al. inferred a MAP of 5–10 mm by comparing their $\Delta^{17}O_{NO_3soil}$ values to a limited amount of pre-existing $\Delta^{17}O_{NO_3soil}$ data. Our new MAP-$\Delta^{17}O_{NO_3soil}$ proxy calibration, however, suggests that the largest $\Delta^{17}O_{NO_3soil}$ value of 14.4‰ arose when the MAP was significantly higher, ~45 mm, not 5–10 mm. The lower $\Delta^{17}O_{NO_3soil}$ values in Rech et al. (2006) were for deep NO_3^-, which may have been formed under even wetter climatic conditions. This reinterpretation is important because the onset of hyper-aridity in the Atacama was suggested to occur in middle Miocene or even later and should have been linked to the uplift of the Andean Cordillera (Hartley et al., 2005; Bissig and Riquelme, 2010). This reinterpretation points to a stepwise aridification rather than a single major climate shift (Reich et al., 2009).

NO_3^- found in the Cambro-Ordovician Nubian sandstone aquifer system in the Hasouna area (Libya) had $\Delta^{17}O$ values between 0.4 and 5‰ (Dietzel et al., 2014). The Nubian sandstone aquifer, one of the world's largest paleo-groundwater aquifers (>2,000,000 km^2), is situated in the Eastern end of the Sahara Desert and consists of fractured quartzitic sandstone that spans 500–1500 m in thickness (see sites in Fig. 1). High contents of NO_3^- (0.47–1.87 mM)

have been found in the Hasouna groundwater for decades, and stable isotope evidence suggested that this groundwater NO_3^- was mainly soil NO_3^- that were flushed from surface soil and not influenced by subsequent denitrification or mixing of *in situ* biotic NO_3^- from nitrification in the aquifer owing to the limited organic matter and dissolved oxygen, respectively (Dietzel et al., 2014). ^{14}C dating indicates this paleo-aquifer was recently recharged at 10 ± 3 ka, after which the recharge is slow under the present arid conditions (Edmunds and Wright, 1979). By using the MAP-$\Delta^{17}O_{NO_3soil}$ model, the ground water $\Delta^{17}O$ values of 0.4–5‰ suggest that this soil-derived NO_3^- originated when MAP was 139.3–200 mm, significantly higher than modern-time MAP in central Libya of ~10 mm (Mamtimin et al., 2011). This higher MAP rate before 10 ± 3 ka agrees with aquifer water isotopes that suggested the Hasouna Nubian Sandstone aquifer recharged during a cooler and more humid climate compared to the current conditions (Sonntag et al., 1978) but failed to infer the magnitude of change in regional MAP.

3.5. Predicting $\Delta^{17}O_{NO_3soil}$ values in other deserts across the globe and the US

The MAP-$\Delta^{17}O_{NO_3soil}$ proxy calibration can also be used to predict $\Delta^{17}O_{NO_3soil}$ values in mid-latitude deserts, by inverting the Eq. (2) to give $\Delta^{17}O_{NO_3soil} = -8.28\ln(MAP) + 45.8$. Global MAP data from http://www.worldclim.org (Hijmans et al., 2005) and high-resolution MAP in the US based on the PRISM model (http://www.prism.oregonstate.edu/) were used in geographic information system (GIS) to generate global middle-latitude and detailed southwestern US $\Delta^{17}O_{NO_3soil}$ isoscapes (Fig. 1). The model predicts that near surface NO_3^- deposits recently found in the Northwestern Badi region of Jordan (Al-Taani and Al-Qudah, 2013), where MAP is between 46 and 96 mm (Al-Ansari and Baban, 2005), would have $\Delta^{17}O_{NO_3soil}$ between 8.0 and 14.1‰. Deposits of NO_3^- found in Israel's southern Negev Desert, which has MAP of $\sim 65 \pm 14$ mm (Rosenthal, 1987), should have $\Delta^{17}O_{NO_3soil}$ values in the range of 9.6–13.2‰. In many deserts, there are scant soil NO_3^- concentration data and even less isotopic data. However, these regions (Australia, North Africa, and others) are likely to have shallow surface NO_3^- deposits with $\Delta^{17}O_{NO_3soil}$ values reflecting local MAP as predicted by the GIS model. Modern-time surface NO_3^- analysis in these regions could be used to further refine the MAP-$\Delta^{17}O_{NO_3soil}$ proxy calibration and test its theoretical underpinnings.

4. Conclusions

It has been demonstrated that there is a strong negative correlation between MAP and $\Delta^{17}O_{NO_3soil}$, and within the MAP range of 11.5–212 mm, $\Delta^{17}O_{NO_3soil}$s can serve as an excellent MAP proxy with $MAP = 253.8 \bullet \exp(-0.12\Delta^{17}O_{NO_3soil})$ ($r^2 = 0.87$). The cause of this correlation is the differences in the relative importance of NO_3^- deposited from the atmosphere and that produced *in situ* by microbial nitrification as precipitation varies. Nitrification becomes dominant when MAP exceeds 210 mm, but scarce when MAP < 11.5 mm. In paleosols and ancient groundwater that were not greatly influenced by aqueous activities and can be accurately dated using radioactive isotopes or other chronologic proxies, the preserved NO_3^- $\Delta^{17}O$ can be used as a paleoprecipitation proxy. The challenge then is finding where such deposits occur in geologic records. We also note that in modern-time soils, spatial and temporal changes in NO_3^- $\Delta^{17}O$ values can be a tracer of biologic nitrogen turnover rates and used to assess nitrogen cycling dynamics.

Acknowledgements

This work was supported by the US National Science Foundation (EAR 0922114) and National Natural Science Foundation of China (40972062). FW was supported by the Purdue Climate Change Research Center Fellowship and Purdue Bilsland Dissertation Fellowship. We thank Brenda Bowen, S.K. Bhattacharya, Raul Ochoa and Ritesh Purohit for assistance during sample collection and Krystin Riha and Wendell Walters during sample isotopic analysis. We also thank the constructive comments from several reviewers.

Appendix A. Supplementary material

Supplementary material related to this article can be found online at http://dx.doi.org/10.1016/j.epsl.2016.01.002.

References

Al-Ansari, N., Baban, S.M., 2005. Rainfall trends in the Badia Region of Jordan. Surv. Land Inf. Sci. 65, 233–243.
Al-Taani, A.A., Al-Qudah, K.A., 2013. Investigation of desert subsoil nitrate in Northeastern Badia of Jordan. Sci. Total Environ. 442, 111–115.
Alexander, B., et al., 2004. Impact of preindustrial biomass-burning emissions on the oxidation pathways of tropospheric sulfur and nitrogen. J. Geophys. Res. 109, D8.
Alexander, B., et al., 2009. Quantifying atmospheric nitrate formation pathways based on a global model of the oxygen isotopic composition (^{17}O) of atmospheric nitrate. Atmos. Chem. Phys. 9, 5043–5056.
Bissig, T., Riquelme, R., 2010. Andean uplift and climate evolution in the southern Atacama Desert deduced from geomorphology and supergene alunite-group minerals. Earth Planet. Sci. Lett. 299 (3), 447–457.
Blaney, H.F., 1957. Evaporation study at Silver Lake in the Mojave Desert, California. EOS, Trans. AGU 38 (2), 209–215.
Böhlke, J.K., Ericksen, G.E., Revesz, K., 1997. Stable isotope evidence for an atmospheric origin of desert nitrate deposits in northern Chile and southern California, USA. Chem. Geol. 136, 135–152.
Böhlke, J.K., Mroczkowski, S.J., Coplen, T.B., 2003. Oxygen isotopes in nitrate: new reference materials for ^{18}O:^{17}O:^{16}O measurements and observations on nitrate-water equilibration. Rapid Commun. Mass Spectrom. 17 (16), 1835–1846.
Boring, L.R., Swank, W.T., Waide, J.B., Henderson, G.S., 1988. Sources, fates, and impacts of nitrogen inputs to terrestrial ecosystems: review and synthesis. Biogeochemistry 6, 119–159.
Buffen, A.M., Hastings, M.G., Thompson, L.G., Mosley-Thompson, E., 2014. Investigating the preservation of nitrate isotopic composition in a tropical ice core from the Quelccaya Ice Cap, Peru. J. Geophys. Res., Atmos. 119, 2674–2697.
Cereceda, P., Schemenauer, R.S., 1991. The occurence of fog in Chile. J. Appl. Meteorol. 30 (8), 1097–1105.
Dietzel, M., et al., 2014. ^{17}O excess traces atmospheric nitrate in paleo-groundwater of the Saharan desert. Biogeosciences 11, 3149–3161.
Dejwakh, N.R., Meixner, T., Michalski, G., McIntosh, J., 2012. Using ^{17}O to investigate nitrate sources and sinks in a semi-arid groundwater system. Environ. Sci. Technol. 46 (2), 745–751.
Edmunds, W.M., Wright, E.P., 1979. Groundwater recharge and palaeoclimate in the Sirte and Kufra basins, Libya. J. Hydrol. 40, 215–241.
Ericksen, G.E., 1981. Geology and origin of the Chilean nitrate deposits. U. S. Geol. Surv. Prof. Pap. 1188. 37 p.
Ewing, S.A., et al., 2007. Rainfall limit of the *N* cycle on Earth. Glob. Biogeochem. Cycles 21, GB3009.
Gleeson, D.B., Herrmann, A.M., Liuesley, S.J., Murphy, D.V., 2008. Influence of water potential on nitrification and structure of nitrifying bacterial communities in semiarid soils. Appl. Soil Ecol. 40, 189–194.
Graham, R.C., Hirmas, D.R., Wood, Y.A., Amrhein, C., 2008. Large near-surface nitrate pools in soils capped by desert pavement in the Mojave Desert, California. Geology 36, 259–262.
Hartley, A.J., Chong, G., Houston, J., Mather, A.E., 2005. 150 million years of climatic stability: evidence from the Atacama Desert, northern Chile. J. Geol. Soc. 162 (3), 421–424.
Hereford, R., Webb, R., Longpré, C., 2006. Precipitation history and ecosystem response to multidecadal precipitation variability in the Mojave Desert region, 1893–2001. J. Arid Environ. 67, 13–34.
Hijmans, R.J., Cameron, S.E., Parra, J.L., Jones, P.G., Jarvis, A., 2005. Very high resolution interpolated climate surfaces for global land areas. Int. J. Climatol. 25, 1965–1978.
Houston, J., 2006a. Evaporation in the Atacama Desert: an empirical study of spatiotemporal variations and their causes. J. Hydrol. 330 (3), 402–412.
Houston, J., 2006b. Variability of precipitation in the Atacama Desert: its causes and hydrological impact. Int. J. Climatol. 26, 2181–2198.

Kaiser, J., Hastings, M.G., Houlton, B.Z., Röckmann, T., Sigman, D.M., 2007. Triple oxygen isotope analysis of nitrate using the denitrifier method and thermal decomposition of N_2O. Anal. Chem. 79, 599–607.

Li, X., Jiang, F., Li, L., Wang, G., 2011. Spatial and temporal variability of precipitation concentration index, concentration degree and concentration period in Xinjiang, China. Int. J. Climatol. 31, 1679–1693.

Lybrand, R.A., Michalski, G., Graham, R.C., Parker, D.R., 2013. The geochemical associations of nitrate and naturally formed perchlorate in the Mojave Desert, California, USA. Geochim. Cosmochim. Acta 104, 136–147.

Mamtimin, B., Et-Tantawi, A.M.M., Schaefer, D., Meixner, F.X., Domroes, M., 2011. Recent trends of temperature change under hot and cold desert climates: comparing the Sahara (Libya) and Central Asia (Xinjiang, China). J. Arid Environ. 75 (11), 1105–1113.

Michalski, G., Bhattacharya, S.K., 2009. The role of symmetry in the mass independent isotope effect in ozone. Proc. Natl. Acad. Sci. USA 106, 5493–5496.

Michalski, G., Böhlke, J.K., Thiemens, M., 2004. Long term atmospheric deposition as the source of nitrate and other salts in the Atacama Desert, Chile: new evidence from mass-independent oxygen isotopic compositions. Geochim. Cosmochim. Acta 68, 4023–4038.

Michalski, G., Scott, Z., Kabiling, M., Thiemens, M.H., 2003. First measurements and modeling of $\Delta^{17}O$ in atmospheric nitrate. Geophys. Res. Lett. 30, 1870.

Miller, M.F., 2002. Isotopic fractionation and the quantification of ^{17}O anomalies in the oxygen three-isotope system: an appraisal and geochemical significance. Geochim. Cosmochim. Acta 66, 1881–1889.

Morin, S., et al., 2009. Comprehensive isotopic composition of atmospheric nitrate in the Atlantic Ocean boundary layer from 65S to 79N. J. Geophys. Res. 114, D05303.

Pluhar, C.J., Kirschvink, J.L., Adams, R.W., 1991. Magnetostratigraphy and clockwise rotation of the Plio-Pleistocene Mojave River formation, central Mojave Desert, California. SBCMA Quarterly 38 (2), 31–42.

Pramanik, S.K., 1952. Hydrology of Rajasthan desert-Rainfall, humidity and evaporation. Bull. Natl. Inst. Sci. India 1, 193–197.

Qin, Y., et al., 2012. Massive atmospheric nitrate accumulation in a continental interior desert, northwestern China. Geology 40, 623–626.

Rech, J.A., Currie, B.S., Michalski, G., Cowan, A.M., 2006. Neogene climate change and uplift in the Atacama Desert, Chile. Geology 34, 761–764.

Reich, M., et al., 2009. Supergene enrichment of copper deposits since the onset of modern hyperaridity in the Atacama Desert, Chile. Miner. Depos. 44 (5), 497–504.

Riha, K.M., 2013. The use of stable isotopes to constrain the nitrogen cycle. PhD dissertation. Purdue University.

Rosenthal, E., 1987. Chemical composition of rainfall and groundwater in recharge areas of the Bet Shean-Harod multiple aquifer system, Israel. J. Hydrol. 89, 329–352.

Seinfeld, J.H., Pandis, S.N., 2006. From Air Pollution to Climate Change: Atmospheric Chemistry and Physics, 2nd edition. John Wiley & Sons, New York.

Sonntag, C., et al., 1978. Paleoclimatic information from deuterium and oxygen-18 in carbon-14 dated north Saharan groundwaters. IAEA SM-228/28:569-581.

Thiemens, M.H., 2006. History and applications of mass-independent isotope effects. Annu. Rev. Earth Planet. Sci. 34, 217–262.

Thompson, R.S., 1991. Pliocene environments and climates in the western United States. Quat. Sci. Rev. 10 (2), 115–132.

United Nations Environment Program (UNEP), 1997. World Atlas of Desertification, 2nd edition. Oxford Press, London, p. 82.

Vicars, W.C., Savarino, J., 2014. Quantitative constraints on the ^{17}O-excess ($\Delta^{17}O$) signature of surface ozone: ambient measurements from 50°N to 50°S using the nitrite-coated filter technique. Geochim. Cosmochim. Acta 135, 270–287.

Walvoord, M.A., et al., 2003. A reservoir of nitrate beneath desert soils. Science 302, 1021–1024.

Wang, F., 2013. The mechanism and timescales of soil formation in the hyper-arid Atacama Desert, Chile. Ph.D. thesis. Purdue University.

Wang, F., Michalski, G., Seo, J.H., Ge, W.S., 2014. Geochemical, isotopic, and mineralogical constraints on atmospheric deposition in the hyper-arid Atacama Desert, Chile. Geochim. Cosmochim. Acta 135, 29–48.

Warren-Rhodes, K., et al., 2006. Hypolithic cyanobacteria, dry limit of photosynthesis, and microbial ecology in the hyperarid Atacama Desert. Microb. Ecol. 52 (3), 389–398.

Winnick, M., Welker, J., Chamberlain, C., 2012. Stable isotopic evidence of El Niño-like atmospheric circulation in the Pliocene Western United States. Clim. Past Discuss. 8 (5), 5083–5108.

Wright, L.A., 1974. Geology of the southeast quarter of the Tecopa quadrangle, San Bernardino and Inyo Counties, California. CDMG Map Sheet 20 (Scale 1:24,000).